ANL-HEP-TR-95-11
STAR NOTE # 196

Efficiency of modified UA1 jet reconstruction algorithm in PP, PA and AA collisions at STAR

B. Christie
Brookhaven National Laboratory

K. Shestermanov[1]
Visitor to Brookhaven National Laboratory from IHEP, Protvino, Russia
Funded in part by High Energy Physics Division Argonne National Laboratory, Argonne, IL 60439

Abstract

The efficiency of a modified *UA1* jet reconstruction algorithm, and the reconstructed jet's P_T resolution in *PP*, *PA* and *AA* events using the **STAR** detector has been studied. The *HIJING* and *PYTHIA* event generators, full *GEANT* simulations and the Time Projection Chamber *(TPC)* Analysis Shell *(TAS)* has been used.

[1]Work supported in part by U.S. Department of Energy, Division of High Energy Physics, Contract W-31-109-ENG-38.

1 Detector

The **STAR** detector at **RHIC** had been described elsewhere [1, 2]. The proposed barrel electromagnetic calorimeter *EMC* [2] is a lead scintillator sampling calorimeter. It covers $|\eta| \leq 1.05$ and 2π in azimuth, thus matching the full tracking acceptance of the *TPC*. The *EMC* segmentation is $\Delta\eta \times \Delta\phi = 0.1$ and it consists of 1200 towers.

2 Event simulation

The *HIJING* [3] event generator has been used for *PP*, *PAu*, *CC*, *OO*, *SiSi* and *FeFe* collisions. In order to compare the jets properties, *PP* events were also simulated using *PYTHIA V5.702/JETSET V7.401 LUND* programs [4].

For the purposes of this study it was desirable to separate the acceptance of the *EMC* barrel from the efficiency of the jet finding code. We accomplished this by calculating the pseudorapidity of the two scattered partons as the events are generated by the *HIJING* event generator code, and only writing out those events for which the scattered partons lie within a prescribed region. For all the results presented in this report both the hard scattered partons were produced within $|\eta| \leq 0.3$.

The initial conditions and kinematics of events of interest have been the following:

- $\sqrt{s} = 200\, GeV$;
- the impact parameter varies from 0 to $0.75\, fm$ for *PAu* and *AA* collisions;
- the P_T of the scattered parton, $P_T^{parton} = 10, 15, 20, 30\, GeV/c$ in *PAu* and $30\, GeV$ in *PP* and *AA* collisions;
- the η_{min} and η_{max} for high $P_T^{partons}$: -0.3 $+0.3$.

The number of events analyzed for each sample of *PP* or *AA* collisions was about 100 and was limited by the *GEANT* computing time and the size of the files created. For example, the processing of 75 *FeFe* events takes about 50 hours of *CPU* on an *rsgi00* processor with $10.5\, Mflops$ and the size of the output files is about $0.3\, Gbyte$.

3 TAS modules for STAR EMC

The package *EMS* (Electro Magnetic Simulation) and the corresponding documentation were created by B. Christie. The brief description below is extracted from *WWW* system of *STAR*, ($STAR \rightarrow STARnews \rightarrow EMC\, news \rightarrow TAS\, ems\, modules$). There are three *TAS* modules in the *EMS* package presently:

1. *ems_tot.F* is the first module called in the ems package. It reads in the *EMC* hits table, which is filled by the *TAS* module *"mct"*, sums up the energy deposited in each of the towers, and fills the output table *"ems_hits_v"*. The input table from *"mct"* contains the *GEANT "hits"* bank information for every charged particle which crosses any plastic layer in the **STAR** *EMC*.

2. *emc_egrid.F* is the second module called in the *EMS* package. This module reads in the output table of *"ems_tot.F"* and the global track table output from the tracking package *"egr"*. For each "good" track in the global track table, this module projects the track to see if it hits the barrel *EMC*. If so, a parameterized amount of energy ($f(\mid P \mid)$) is subtracted from the struck tower. The track is then projected in the other direction to the point of closest approach to the primary vertex. At present the primary vertex is assumed to be at coordinates 0,0,0. The tracks total energy is evaluated at this point, assuming that it is a pion, and this "charged" energy is put into the appropriate $\eta - \phi$ bin. After this the energy remaining in the *EMC* barrel is multiplied by 1/sampling factor (= 16.00) to give the deduced neutral energy incident on the *EMC*. This factor of 16.00 is set via a data statement in the module. The output table for this module is named *"eme_cor"*.

3. *erj_bar.F* is the third module called in the *EMS* package. This module contains the modified (by K. Shestermanov) *UA1* jet finding code. This module reads in the output table of the *"emc_egrid"* module described above.

4 Results

The modified *UA1* algorithm [5, 6, 7] has been used for jet finding. This is a cone type algorithm, and it has 3 parameters:

- The tower threshold for seed transverse energy, E_T^{seed};
- The jet cone radius in $\eta - \phi$ plane, R_0;
- The threshold for jet energy, E_j.

For our study the algorithm has been modified in order to suppress the background from soft interactions in AA collisions.

It proceeds through the following steps:

1. Each cell in the energy histogram $\eta - \phi$ is assigned an energy vector whose magnitude is given by the energy deposited in the cell, E_T, and whose direction is given by the center of the cell.

2. The average transverse energy per cell, E_{back}, is calculated ($E_{back} = \frac{1}{n}\sum_{i,j} E_{i,j}$, where n is the number of cells). Then, this value is subtracted from each cell.

3. All cells with $E_T > E_T^{seed}$ are ordered in decreasing transverse energy.

4. The cell with the highest transverse energy initiates the first jet.

5. Cells are added vectorially to the first one if they are within a distance R_0 (in $\eta - \phi$ space) from the center of a cone at the cell with the highest E_T. A jet momentum vector is defined as the vectorial sum of all individual cells within the cone of radius R_0. The center of the cone is then recalculated in the direction of the reconstructed jet momentum. This procedure is repeated until the distance between the 'old' and 'new' center of the cone becomes less then $0.05 \cdot R_0$.

6. If the next seed cell is outside this radius then a new jet is initiated. This procedure is repeated until all cells above E_T^{seed} threshold are assigned to jets.

7. If the jet energy is greater than E_j the jet is accepted.

8. The value E_{back} of the background E_T energy is then recalculated using only remaining cells not assigned to the jets, and the jet finding iteration is repeated.

This algorithm converges in three-four steps.
The efficiency of two jet finding is defined as

$$Eff = N_{dijets}/N_{dipartons} \ ,$$

where N_{dijets} is the number of events with two jets; $N_{dipartons}$ is the number of generated events with two high P_T partons with the kinematics described earlier.

The jets were considered to be found if back-to-back ϕ deviations for the two jets don't exceed $30°$, and the jet's energy was greater than $10\,GeV$ (N.B. this cut is only used for the study of $30\,GeV$ jets). We checked the angular correlation between the scattered parton and the reconstructed jets. In the case of *PP* the average value for the deviation in ϕ was $\simeq 5°$. In *FeFe* the average value for this deviation was $\simeq 13°$.

The results for efficiencies and for the $RMS\ P_T^{jet}$ value for $R_0 = 1$, $E_j = 5\,GeV$ ($E_j = 9\,GeV$ in *FeFe* collisions) and $E_T^{seed} = 1.0\,GeV$ are presented in table 1 and fig. 1.

Table 1. Efficiencies and $RMS\ P_T^{jet}$.

Interaction	Efficiency, %	$RMS\ P_T^{jet}$, %
PP(HIJING)	78.9 ± 8.0	24.1
PAu	63.8 ± 7.8	30.8
CC	65.8 ± 6.5	30.4
OO	70.7 ± 7.3	30.3
SiSi	61.3 ± 9.0	30.9
FeFe	47.9 ± 7.1	38.7

The distribution of the differences between P_T^{parton} and P_T^{jet} in *PP*, *PAu* and *AA* collisions are shown in figs. 2-7.

Note that the mean of the distributions of $P_T^{parton} - P_T^{jet}$ get more positive as the size of the colliding systems increases. This may be a consequence of the jet quenching mechanism in *HIJING*. This jet quenching leads to a softening and broadening of the fragmentation function via induced gluon bremsstrahlung for the high P_T partons. As the fragmentation function broadens more of the jet's energy falls outside of the fixed cone radius used in the jet algorithm. This is consistent with the trend shown in figs. 2-7. We will investigate this further by generating events with the jet quenching feature turned off in *HIJING*.

The results for efficiencies and for the $RMS\ P_T^{jet}$ values as a function of P_T^{jet} in the *PAu* collisions are presented in fig. 8 for $E_T^{seed} = 0.5\,GeV$, $E_j = 3\,GeV$, and the same demands for angles in the XY plane. No additional cut for the jet's energy has been applied.

To determine quantitatively how the finite resolution, tracking efficiency, and pixelation of the **STAR** detector affects our jet finding efficiency and resolution, the jet finding algorithm was run directly on the output of the event generators. In this study the jet direction was taken to be the direction of the scattered parton, as given by the event generator. The energy of all particles in the event generator output file (excluding neutrinos) which were within the cone radius of the parton was summed to get the jet energy. The results for PP collisions ("ideal") are presented in table 2.

Table 2. Parameters of jets from different event generators in PP collisions.

	HIJING		PYTHIA	
	"ideal"	STAR	"ideal"	STAR
Efficiency, %		78.9 ± 8.0		91.9 ± 8.6
$P_T^{parton}\,(RMS)$, GeV/c	30.3(2.4)	30.3(2.3)	30.5(1.5)	30.4(1.6)
$P_T^{jet}\,(RMS)$, GeV/c	25.2(5.5)	24.8(5.9)	26.6(4.1)	26.7(6.3)
Angle in YZ plane (RMS), *degree*	11.5(11.8)	13.6(14.6)	3.1(5.0)	3.9(6.5)
Angle in space (RMS), *degree*	13.8(12.0)	16.1(15.3)	4.9(7.4)	6.5(10.2)

From this table one observes that the data for both **STAR** and the "ideal" detector are quite close to one another. The small differences observed are primarily due the inefficiency of the *STAR* detector to the neutrons and K_L^0 mesons, and also from the finite resolution and granularity of the **STAR** calorimeter.

Much more significant are the differences of the angles between the parton and jet axis for the events generated with *HIJING* and *PYTHIA*. The *HIJING* events show a much wider distribution for this quantity than the *PYTHIA* events. It is important that we understand the reason for this difference as it has a direct impact on our resolution of the Bjorken x values in our analysis.

For comparison purposes we empirically extracted the charged particle fragmentation function for the *HIJING* and *PYTHIA* event generators. One can see this in fig. 9, where the charged particle fragmentation functions for $P_T = 30\,GeV/c$ jets are shown as a function of the inclusive variable [8]

$$z = P_l^{\pm}/E_{parton}\,,$$

where $P_l^{\pm}$ is the momentum of the charged particle projected on the parton axis, and E_{parton} is the energy of the parton.

5 Conclusion

It has been shown that the modified *UA1* jet finding algorithm can be used with reasonable efficiency for jet reconstruction in the central η region in *PP*, *PA*, and heavy ions collisions. Still to be understood and resolved is some inconsistency of the characteristics of the *PP* events produced by the *HIJING* and *PYTHIA/JETSET* generators.

The discussions with A. Yokosawa, J. Carroll, G. Westfall, D. Underwood, T. Hallman and V. Rykov were extremely helpful. We appreciate all of them.

References

[1] *The STAR collaboration*, Conceptual Design Report for the Solenoidal Tracker at RHIC (STAR), June 15, 1992.

[2] *The STAR EMC collaboration*, Conceptual Design Report for the Electromagnetic Calorimeter for the **STAR**, September 22, 1993.

[3] Miklos Gyulassy and Xin-Nian Wang, LBL-34246 (1994)

[4] T.Sjostrand, CERN-TH. 7112/93 (1993)

[5] Arnison et al., (UA1 Collaboration), Phys. Lett., **132B**,214(1983)

[6] B. Flaugher and K. Meier, FERMILAB-Conf-90/248-E,1990.

[7] V. Korotkikh et al., Preprint INP MSU 94-30/352, 1994.

[8] Arnison et al., (UA1 collaboration), Phys. Lett., **132B**,223(1983)

Figure Captions

Fig. 1. Efficiency of finding dijets and RMS P_T^{jet} resolution in PP, PAu and AA interactions.

Fig. 2. $P_T^{parton} - P_T^{jet}$ distribution in PP interactions.

Fig. 3. $P_T^{parton} - P_T^{jet}$ distribution in PAu interactions.

Fig. 4. $P_T^{parton} - P_T^{jet}$ distribution in CC interactions.

Fig. 5. $P_T^{parton} - P_T^{jet}$ distribution in OO interactions.

Fig. 6. $P_T^{parton} - P_T^{jet}$ distribution in $SiSi$ interactions.

Fig. 7. $P_T^{parton} - P_T^{jet}$ distribution in $FeFe$ interactions.

Fig. 8. Efficiency of finding dijets and RMS P_T^{jet} resolution in PAu interactions as function of P_T^{jet}.

Fig. 9. Charged-particle fragmentation function for $P_T^{jet} = 30\,GeV/c$ in PP interactions for $HIJING$(shadow) and $PYTHIA$ event generators.

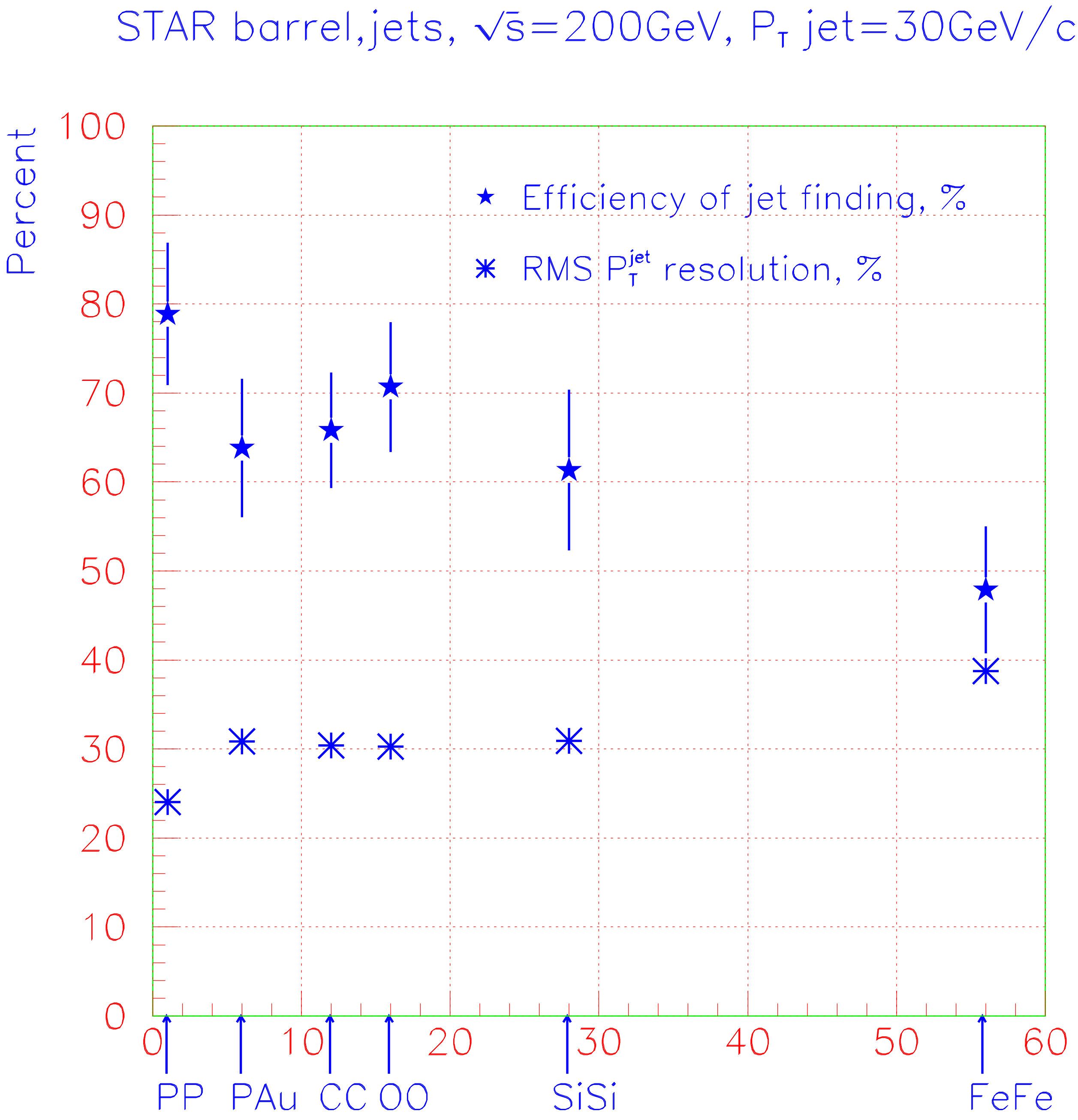
STAR barrel,jets, √s=200GeV, P_T jet=30GeV/c
Percent
100
90
80
70
60
50
40
30
20
10
0
0
10
20
30
40
50
60
Efficiency of jet finding, %
RMS P_T^jet resolution, %
PP
PAu
CC
OO
SiSi
FeFe
Fig. 1

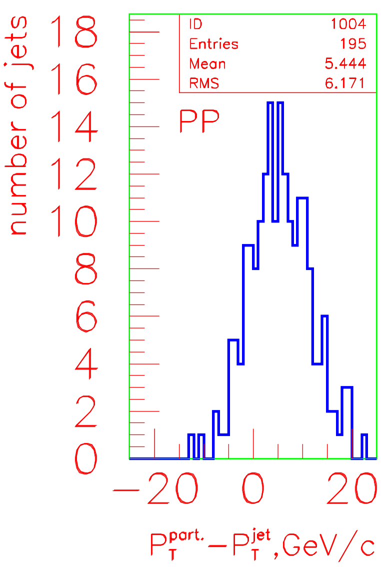

Fig. 2

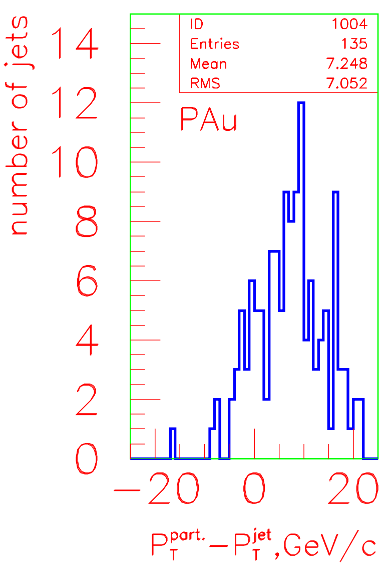

Fig. 3

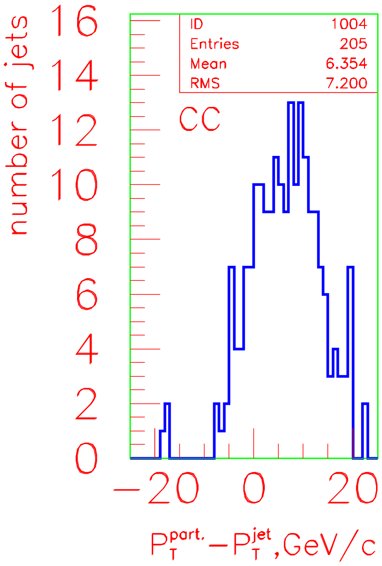

Fig. 4

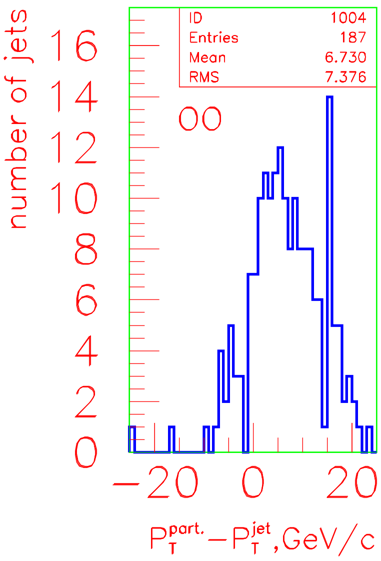

Fig. 5

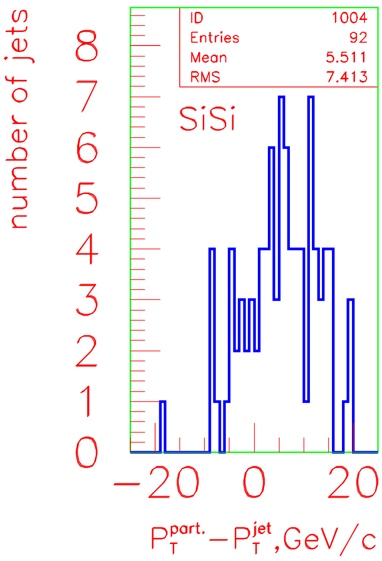

Fig. 6

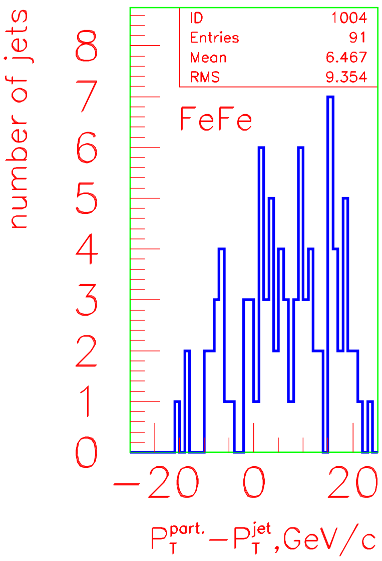

Fig. 7

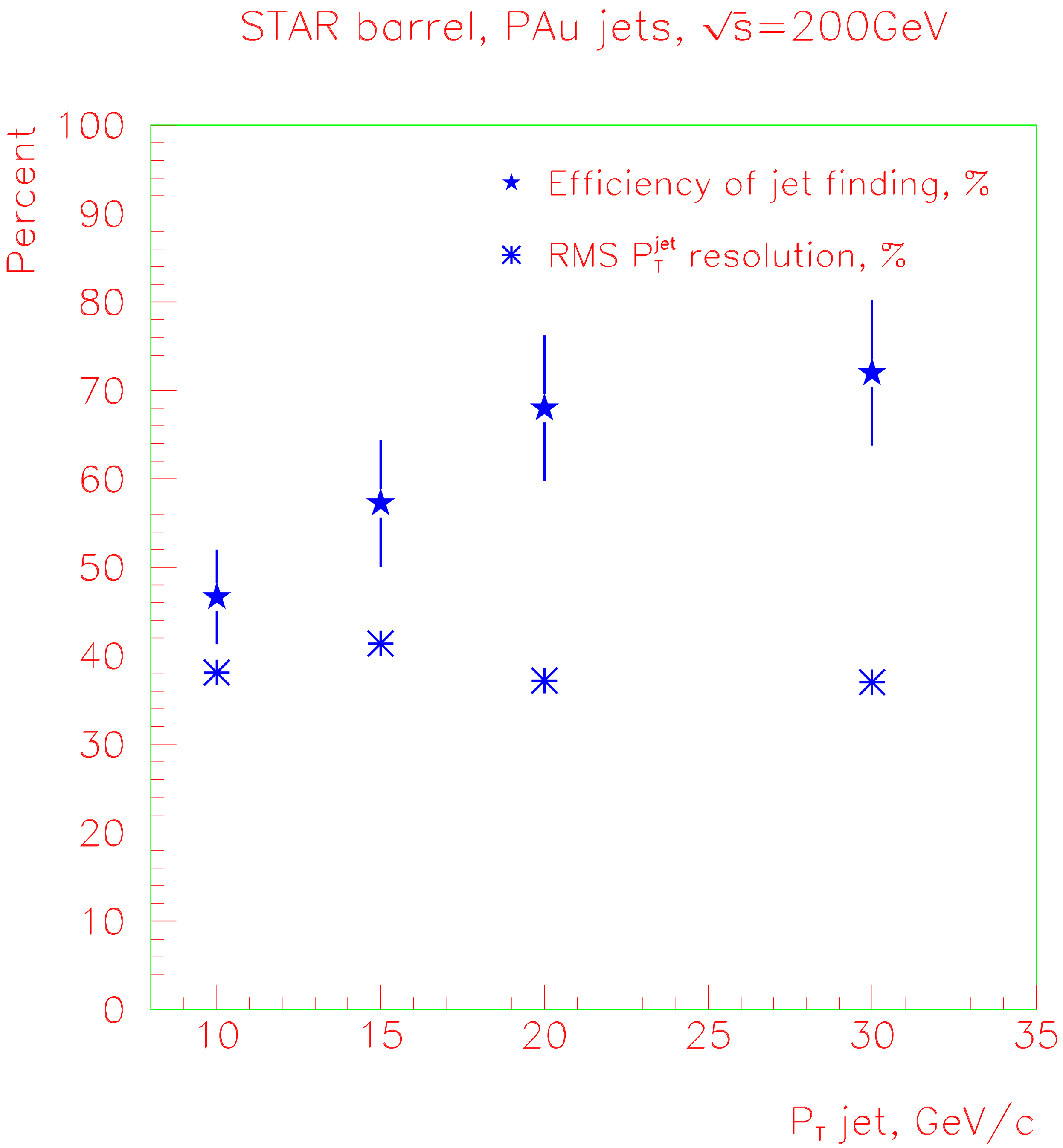
STAR barrel, PAu jets, √s=200GeV
Percent
Efficiency of jet finding, %
RMS P_T^{jet} resolution, %
P_T jet, GeV/c
0
10
20
30
40
50
60
70
80
90
100
10
15
20
25
30
35

Fig. 8

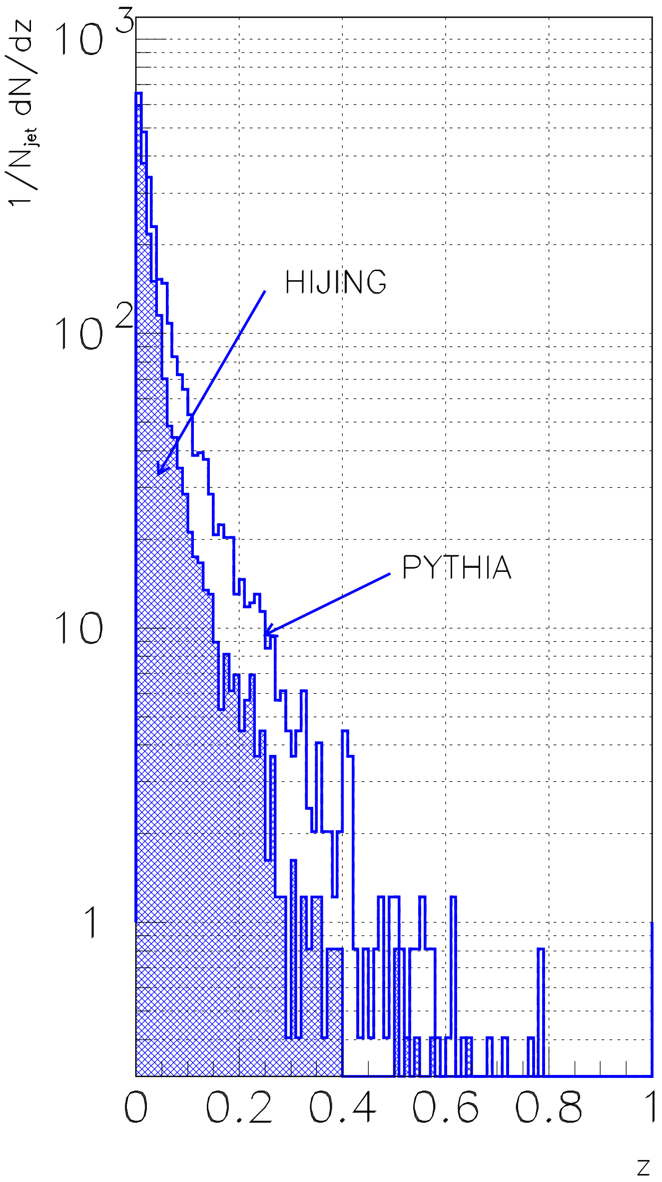

Fig. 9